Research Article Vol. 32, No. 27 / 30 Dec 2024 / Optics Express 48645
Optics EXPRESS

Fourier coupled modal method for parallel modal analysis of photonic structures

JONGHYUN LEE,[1] MYEONGGYU CHOI,[1] SEHYEON JEONG,[1] SHIN-WOONG PARK,[2] AND HWI KIM[1,*]

[1]Department of Electronics and Information Engineering, Colledge of Science and Technology, Korea University, Sejong Campus, 2511 Sejong-ro, Sejong 30019, Republic of Korea
[2]Center for Advanced Photovoltaic Materials (CAPM), Korea University, Sejong Campus, 2511 Sejong-ro, Sejong 30019, Republic of Korea
*hwikim@korea.ac.kr

Abstract: We present the Fourier coupled modal method (FCMM) as a solution for large-scale photonic structure analysis, emphasizing its inherent parallelism, facilitated by spatial partitioning and Fourier modal field computation. The parallelism of the FCMM is achieved by integrating the coupled mode theory (CMT) within the Fourier modal method (FMM). The proposed numerical framework of the FCMM is detailed and validated through a comparative study with the conventional FMM.

1. Introduction

Computational photonics is integral to the design and analysis of photonics devices and systems. Photonic component design requires electromagnetic simulation and modal analysis of passive and active complex photonic structures over a wide range of wavelengths. As a foundational technology, computational photonics has seen significant progress with advancement in computational technology. Over the past few decades, notable innovations have emerged in established computational photonics methods including finite difference time domain (FDTD) [1], finite element method (FEM) [2,3], and Fourier modal method (FMM) [4–7]. These methods have been distributed as commercialized simulation tools or free open-source codes, becoming critical tools for designing and analyzing state-of-the-art photonic devices. As device scale increases, computation resources must increase accordingly, and most of the methods face limitations when applied to large-scale photonic structures. A few approximation methods to reduce computational resource demands in electromagnetic field calculations are based on the effective medium theory (EMT) [16–18]. EMT can reduce computational complexity, however, its application is limited for large-area photonic structures featuring highly multimodal dynamics and inhomogeneous permittivity profiles. To overcome those hurdles, parallel computation has been considered an essential research topic for most methods [8]. Nevertheless, employing parallel computing systems necessitates specialized parallel algorithms to accelerate and expand the computational capability in most of the computational photonics methods.

Fourier modal method (FMM), a widely-used frequency-domain technique in computational photonics, is fundamentally based on modal analysis. It is particularly effective for analyzing diffractive and scattering structures, including gratings, metamaterials, meta-surfaces, and photonic waveguide structures. The development of computational parallelism for FMM is an ongoing and critical challenge; however, notably, there remains a lack of both theoretical and practical implementations FMM in parallel computing systems. In the central part of FMM, a large-scale eigenvalue problem of a general non-symmetric, non-Hermitian complex matrix exists. Unfortunately, the efficient parallel algorithm for this general complex eigenvalue problem is still unsolved [9,10], meaning that the lateral parallelism of FMM, necessary to model large-scale

#545717 https://doi.org/10.1364/OE.545717
Journal © 2024 Received 23 Oct 2024; revised 23 Nov 2024; accepted 4 Dec 2024; published 20 Dec 2024

Optics EXPRESS

photonic structures, remains underdeveloped and poorly understood. In the conventional FMM framework, the lateral parallelism is currently infeasible.

In this paper, we introduce a novel approach to parallelize FMM, referred to as the Fourier coupled modal method (FCMM). The proposed FCMM framework is formulated in the form of the zero-gap coupled mode theory (zero-gap CMT) based on FMM. The core idea of the FCMM is the dimensional reduction of the large-scale eigenvalue problem into several reduced-dimension eigenvalue problems corresponding to the global modal analysis of CMT, which leads to the large-scale Fourier modal analysis of photonic structures.

Our focus extends beyond simply determining the electromagnetic field distribution in large-scale photonic structures, but we want to seek an approach that facilitates the modal analysis of energy exchange between optical modes within the investigated structures. The proposed FCMM has a strong advantage over FDTD and FEM in this aspect. The capability of the modal analysis enables the large-scale photonic analysis featuring parallel computation. Using zero-gap CMT, the spatial partitioning of the photonic structure is modeled. In this scheme, the mutual interaction for energy transfer among multiple coupled modes is calculated to obtain optical field distribution through the superposition of eigenmodes of decomposed interacting media [11–14]. The phenomenon of the near-field mode coupling between adjacent localized structures plays a crucial role in explaining various optical phenomena such as propagation, transmission/reflection, diffraction, scattering, and energy exchange. This work demonstrates the parallelism of the FCMM and its applicability in the two-dimensional representations and for the bounded modes of simple multi-slab waveguide systems. The developed FCMM scheme can be readily extended to analyze three-dimensional structures.

2. FCMM models of structure and optical field

The permittivity profile of the target structure is assumed to be described by $\varepsilon(x)$ with no variation in the z-direction as seen in Fig. 1(a). Spatial partitioning is applied to $\varepsilon(x)$, dividing it into P local parts $\varepsilon^{(1)}(x)$ $\varepsilon^{(2)}(x)$ $\cdots$ $\varepsilon^{(P)}(x)$ as illustrated in Fig. 1(b). The target structure $\varepsilon(x)$ consists of a collection of local permittivity functions, $\varepsilon = \begin{pmatrix} \varepsilon^{(1)} & \varepsilon^{(2)} & \cdots & \varepsilon^{(P)} \end{pmatrix}$. As shown in Fig. 1(c), each local part is embedded within a homogeneous medium with permittivity ε_s. The permittivity profile is expressed as:

$$\bar{\varepsilon}^{(p)}(x) = \begin{cases} \varepsilon^{(p)}(x) & \text{for } x \in W_p \\ \varepsilon_s & \text{for } x \notin W_p \end{cases}. \tag{1}$$

In CMT, the positive and negative Bloch eigenmodes of the p-th part are represented by

$$\begin{pmatrix} E_p^+ \\ H_p^+ \end{pmatrix} = \sum_{v=1}^{N} A_v^{(p)+}(z) \begin{pmatrix} E_v^{(p)+}(x) \\ H_v^{(p)+}(x) \end{pmatrix} e^{\alpha_v^{(p)+}(z-z_-)} e^{j\beta_v^{(p)+}(z-z_-)} = \sum_{v=1}^{N} C_v^{(p)+}(z) \begin{pmatrix} E_v^{(p)+}(x) \\ H_v^{(p)+}(x) \end{pmatrix} e^{j\beta_v^{(p)+}(z-z_-)}, \tag{2a}$$

$$\begin{pmatrix} E_p^- \\ H_p^- \end{pmatrix} = \sum_{v=1}^{N} A_v^{(p)-}(z) \begin{pmatrix} E_v^{(p)-}(x) \\ H_v^{(p)-}(x) \end{pmatrix} e^{\alpha_v^{(p)-}(z-z_+)} e^{j\beta_v^{(p)-}(z-z_+)} = \sum_{v=1}^{N} C_v^{(p)-}(z) \begin{pmatrix} E_v^{(p)-}(x) \\ H_v^{(p)-}(x) \end{pmatrix} e^{j\beta_v^{(p)-}(z-z_+)}, \tag{2b}$$

where $E_v^{(p)\pm}(x)$ and $H_v^{(p)\pm}(x)$ represent the transverse modal profiles, and p denotes the local index. P is the number of waveguides, and N is the number of the eigenmodes of a single waveguide. The eigenvalue, corresponding to the propagation constant, is $\alpha_v^{(p)\pm} + j\beta_v^{(p)\pm}$. Let $C_v^{(p)\pm}$ be the coupling coefficient function defined by $C_v^{(p)\pm} = A_v^{(p)\pm} e^{\alpha_v^{(p)\pm}(z-z_\mp)}$. The coupling coefficient $C_v^{(p)\pm}$ is set to contain a real part of the complex eigenvalue $\alpha_v^{(p)\pm}$, which is the key factor for numerical

Optics EXPRESS

stability of the FCMM. In the Bloch eigenmode representation of Eqs. (2a) and (2b). the terms of $E_v^{(p)\pm}(x)e^{j\beta_v^{(p)\pm}(z-z_\mp)}$ and $H_v^{(p)\pm}(x)e^{j\beta_v^{(p)\pm}(z-z_\mp)}$ are stable, showing neither damping nor divergence along the z-axis. The coupling coefficients $C_v^{(p)\pm}$ account for the damping and divergence effects of the eigenmodes in the z-axis. This formulation ensures the numerical stability of FCMM.

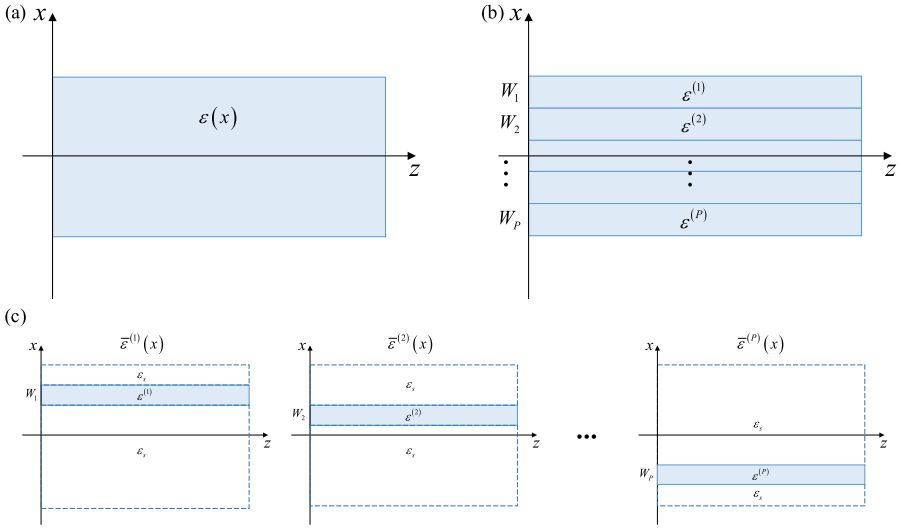

Fig. 1. Schematic representation of the Fourier coupled modal method (FCMM) structure: (a) the total structure, (b) the partitioned structure, and (c) the individually shifted structure.

The computational domain configuration is depicted in Fig. 2. The entire space in Fig. 2(a) is split into multiple sub-domains shown in Fig. 2(b). For instance, Fig. 2 shows the spatial partitioning scheme, in which the entire space is divided into 5×1 sub-domains. The sub-domain is surrounded by buffer that is a homogeneous medium with permittivity ε_s. Independent FMM analysis is conducted for the local parts in the sub-domains of Fig. 2(b) to obtain the Bloch eigenmodes, $E_v^{(p)\pm}(x)$ and $H_v^{(p)\pm}(x)$ with $\alpha_v^{(p)\pm} + j\beta_v^{(p)\pm}$. The spatial partitioning allows the original large-scale eigenvalue problem to be decomposed into multiple smaller eigenvalue problems.

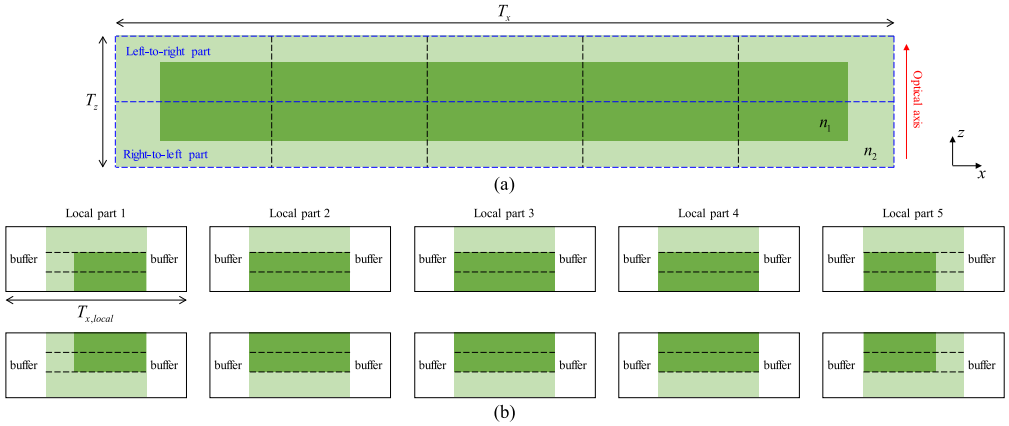

Fig. 2. Numerical scheme of bidirectional FCMM structures (5 by 1 localization): (a) the global structure within the global domain, and (b) the segmented structures within the local domain for left-to-right (upper) and right-to-left (lower) incident directions.

Optics EXPRESS

According to coupled mode theory (CMT), when P local waveguides are combined to form a complete structure $\varepsilon(x)$, the total field supported by the structure $\varepsilon(x)$ is expressed as:

$$\begin{pmatrix} \tilde{E}^{\pm} \\ \tilde{H}^{\pm} \end{pmatrix} = \sum_{p=1}^{P} \left[\sum_{v=1}^{N} C_v^{(p)\pm}(z) \begin{pmatrix} E_v^{(p)\pm}(x) \\ H_v^{(p)\pm}(x) \end{pmatrix} e^{j\beta_v^{(p)\pm}(z-z_{\mp})} \right] = \sum_{p=1}^{P} \left[\sum_{v=1}^{N} C_v^{(p)\pm}(z) \begin{pmatrix} \tilde{E}_v^{(p)\pm}(x) \\ \tilde{H}_v^{(p)\pm}(x) \end{pmatrix} \right], \quad (3a)$$

where the local modes $\tilde{E}_v^{(p)\pm}$ and $\tilde{H}_v^{(p)\pm}$ are given by

$$\begin{pmatrix} \tilde{E}_v^{(p)\pm} \\ \tilde{H}_v^{(p)\pm} \end{pmatrix} = \begin{pmatrix} E_v^{(p)\pm} \\ H_v^{(p)\pm} \end{pmatrix} e^{j\beta_v^{(p)\pm}(z-z_{\mp})}, \quad (3b)$$

$$\begin{pmatrix} E_v^{(p)\pm} \\ H_v^{(p)\pm} \end{pmatrix} = \sum_{m=-M}^{M} \begin{pmatrix} E_{v,x,m}^{(p)\pm} & E_{v,y,m}^{(p)\pm} & E_{v,z,m}^{(g)\pm} \\ H_{v,x,m}^{(g)\pm} & H_{v,y,m}^{(g)\pm} & H_{v,z,m}^{(g)\pm} \end{pmatrix} e^{jk_{x,m}x}. \quad (3c)$$

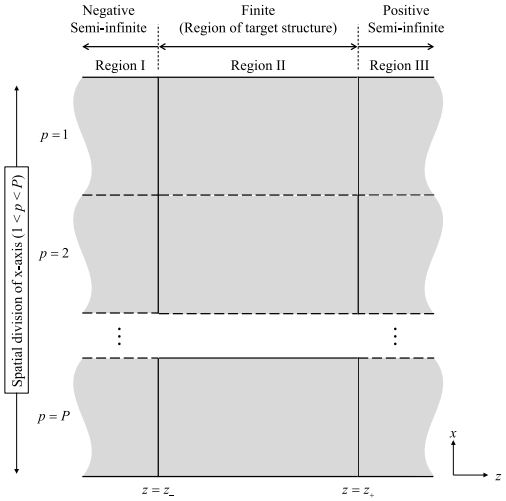

Fig. 3. The total space of the FCMM field distribution, consisting of negative semi-infinite region I, finite region II (target structure), and positive semi-infinite region III.

Equation (3a) is referred to FCMM field representation. In the FCMM, the field distribution of the local mode is defined across the entire space in Fig. 3. The local eigenmode of Eq. (3c) represents the fundamental form of the FMM-field representation. The detailed field model of FCMM is outlined in Supplement 1 section A. Using the CMT described in Supplement 1 section B, the differential equation system for the mode coupling (MC) operator functions $C_v^{(p)\pm}(z)$ is derived as

$$\sum_{p=1}^{P} \sum_{v=1}^{N} M_{\mu,v}^{q,p,\pm} \frac{dC_v^{(p)\pm}(z)}{dz} = \sum_{p=1}^{P} \sum_{v=1}^{N} [H_{\mu,v}^{q,p,\pm} + \alpha_v^{(p)\pm} M_{\mu,v}^{q,p,\pm}] C_v^{(p)\pm}(z) \text{ for} 1 \le q \le P, 1 \le \mu \le N. \quad (4)$$

where $M_{\mu,v}^{q,p,\pm}$ and $H_{\mu,v}^{q,p,\pm}$ represents the overlap integrals defined respectively as

$$M_{\mu,v}^{q,p,\pm} = \int u_z [\tilde{E}_v^{(p)\pm}(x) \times \tilde{H}_{\mu}^{*(q)\pm}(x) + \tilde{E}_{\mu}^{*(q)\pm}(x) \times \tilde{H}_v^{(p)\pm}(x)] dx, \quad (5a)$$

Optics EXPRESS

$$H_{\mu,v}^{q,p,\pm} = j\omega\varepsilon_0 \int (\varepsilon - \varepsilon^{(p)})\tilde{E}_v^{(p)\pm}(x) \cdot \tilde{E}_\mu^{*(q)\pm}(x)dx. \tag{5b}$$

$M_{\mu,v}^{q,p,\pm}$ corresponds to the z-directional cross-modal Poynting power and $H_{\mu,v}^{q,p,\pm}$ represents the mode coupling strength. The equation for the MC operator functions $C_v^{(p)\pm}(z)$ is structured as the $PN \times PN$ differential equations:

$$\begin{pmatrix} d\underline{C}^{(1)\pm} \\ d\underline{C}^{(2)\pm} \\ d\underline{C}^{(3)\pm} \\ \vdots \\ d\underline{C}^{(P)\pm} \end{pmatrix} = \begin{pmatrix} \mathbf{M}_\pm^{1,1} & \mathbf{M}_\pm^{1,2} & \mathbf{M}_\pm^{1,3} & & \\ \mathbf{M}_\pm^{2,1} & \mathbf{M}_\pm^{2,2} & \mathbf{M}_\pm^{2,3} & & \\ \mathbf{M}_\pm^{3,1} & \mathbf{M}_\pm^{3,2} & \mathbf{M}_\pm^{3,3} & & \\ & & & \ddots & \\ & & & & \mathbf{M}_\pm^{P,P} \end{pmatrix}^{-1} \times$$
$$\begin{pmatrix} \mathbf{H}_\pm^{1,1} + \alpha_\pm^{(1)\pm}\mathbf{M}_\pm^{1,1} & \mathbf{H}_\pm^{1,2} + \alpha_\pm^{(2)\pm}\mathbf{M}_\pm^{1,2} & \mathbf{H}_\pm^{1,3} + \alpha_\pm^{(3)\pm}\mathbf{M}_\pm^{1,3} & & \\ \mathbf{H}_\pm^{2,1} + \alpha_\pm^{(1)\pm}\mathbf{M}_\pm^{2,1} & \mathbf{H}_\pm^{2,2} + \alpha_\pm^{(2)\pm}\mathbf{M}_\pm^{2,2} & \mathbf{H}_\pm^{2,3} + \alpha_\pm^{(3)\pm}\mathbf{M}_\pm^{2,3} & & \\ \mathbf{H}_\pm^{3,1} + \alpha_\pm^{(1)\pm}\mathbf{M}_\pm^{3,1} & \mathbf{H}_\pm^{3,2} + \alpha_\pm^{(2)\pm}\mathbf{M}_\pm^{2,3} & \mathbf{H}_\pm^{3,3} + \alpha_\pm^{(3)\pm}\mathbf{M}_\pm^{3,3} & & \\ & & & \ddots & \\ & & & & \mathbf{H}_\pm^{P,P} + \alpha_\pm^{(P)\pm}\mathbf{M}_\pm^{P,P} \end{pmatrix} \begin{pmatrix} \underline{C}^{(1)\pm} \\ \underline{C}^{(2)\pm} \\ \underline{C}^{(3)\pm} \\ \vdots \\ \underline{C}^{(P)\pm} \end{pmatrix}, \tag{5c}$$

This differential equation system of $C_v^{(p)\pm}(z)$ can be numerically solved using the fourth-order Runge-Kutta algorithm. The z-dependent coupling coefficient functions $C_v^{(p)\pm+}(z)$ are collectively represented by the mode coupling (MC) matrix operator (Supplement 1 section C). The positive MC operator $\mathbf{\Gamma}^+(z)$ and negative MC operator $\mathbf{\Gamma}^-(z)$ are expressed as:

$$\begin{pmatrix} \underline{C}^{(1)+}(z) \\ \underline{C}^{(2)+}(z) \\ \vdots \\ \underline{C}^{(P)+}(z) \end{pmatrix} = \begin{pmatrix} \mathbf{C}^{(1,1)+}(z) & \mathbf{C}^{(1,2)+}(z) & \cdots & \mathbf{C}^{(1,P)+}(z) \\ \mathbf{C}^{(2,1)+}(z) & \mathbf{C}^{(2,2)+}(z) & & \mathbf{C}^{(2,P)+}(z) \\ \vdots & \vdots & \ddots & \vdots \\ \mathbf{C}^{(P,1)+}(z) & \mathbf{C}^{(P,2)+}(z) & \cdots & \mathbf{C}^{(P,P)+}(z) \end{pmatrix} \begin{pmatrix} \underline{C}^{(1)+}(z_-) \\ \underline{C}^{(2)+}(z_-) \\ \vdots \\ \underline{C}^{(P)+}(z_-) \end{pmatrix} = \mathbf{\Gamma}^+(z)C^+(z_-) \text{ at } z_- \le z \le z_+, \tag{6a}$$

$$\begin{pmatrix} \underline{C}^{(1)-}(z) \\ \underline{C}^{(2)-}(z) \\ \vdots \\ \underline{C}^{(P)-}(z) \end{pmatrix} = \begin{pmatrix} \mathbf{C}^{(1,1)-}(z) & \mathbf{C}^{(1,2)-}(z) & \cdots & \mathbf{C}^{(1,P)-}(z) \\ \mathbf{C}^{(2,1)-}(z) & \mathbf{C}^{(2,2)-}(z) & & \mathbf{C}^{(2,P)-}(z) \\ \vdots & \vdots & \ddots & \vdots \\ \mathbf{C}^{(P,1)-}(z) & \mathbf{C}^{(P,2)-}(z) & \cdots & \mathbf{C}^{(P,P)-}(z) \end{pmatrix} \begin{pmatrix} \underline{C}^{(1)-}(z_+) \\ \underline{C}^{(2)-}(z_+) \\ \vdots \\ \underline{C}^{(P)-}(z_+) \end{pmatrix} = \mathbf{\Gamma}^-(z)C^-(z_+), \text{ at} z_- \le z \le z_+. \tag{6b}$$

where $\underline{\mathbf{C}}^{(p)\pm}(z_\mp)$ represents the left and right-end boundary condition at $z = z_\mp$, and $\underline{\mathbf{C}}^{(p)\pm}(z)$ denotes z-dependent matrix function. The off-diagonal elements in the MC operators describe the mutual cross-coupling dynamics of eigenmodes.

3. FCMM single block scattering matrix operator

Let us assume that the total space is divided into three regions; left semi-infinite region I, finite region II, and right semi-infinite region III. Each region has its own FCMM fields. The total field

Optics EXPRESS

distribution in the entire space is represented as

$$\begin{pmatrix}\tilde{E}\\ \tilde{H}\end{pmatrix}=\begin{cases}\sum_{p=1}^{P}\sum_{\nu=1}^{N}C_{I,\nu}^{(p)\pm}(z)\begin{pmatrix}E_{I,\nu}^{(p)\pm}(x)\\ H_{I,\nu}^{(p)\pm}(x)\end{pmatrix}e^{j\beta_{I,\nu}^{(p)\pm}(z-z_-)} & \text{for } z<z_-\\ \sum_{p=1}^{P}\sum_{\nu=1}^{N}C_{II,\nu}^{(p)+}(z)\begin{pmatrix}E_{II,\nu}^{(p)+}(x)\\ H_{II,\nu}^{(p)+}(x)\end{pmatrix}e^{j\beta_{II,\nu}^{(p)+}(z-z_-)}+\sum_{p=1}^{P}\sum_{\nu=1}^{N}C_{II,\nu}^{(p)-}(z)\begin{pmatrix}E_{II,\nu}^{(p)-}(x)\\ H_{II,\nu}^{(p)-}(x)\end{pmatrix}e^{j\beta_{II,\nu}^{(p)-}(z-z_+)} & \text{for } z_-\le z\le z_+\\ \sum_{p=1}^{P}\sum_{\nu=1}^{N}C_{III,\nu}^{(p)+}(z)\begin{pmatrix}E_{III,\nu}^{(p)+}(x)\\ H_{III,\nu}^{(p)+}(x)\end{pmatrix}e^{j\beta_{III,\nu}^{(p)+}(z-z_+)} & \text{for } z_+\le z\end{cases} \tag{7}$$

The optical field propagation process consists of two distinct steps. The first involves reflection and transmission at the left and right interfaces, while the second concerns mode-coupling governed by the CMT (Supplement 1 section C).

A key component is the scattering matrix operator for a finite size single block in region II. To define the scattering-matrix of a finite single-block with the left and right boundaries, the local boundary scattering matrix (S-matrix) operators of each local part at the interfaces $z = z_-$ and $z = z_+$ are constructed as in Fig. 4. The bidirectional boundary S-matrix operators are derived from local FMM analysis and those are used to construct the total single-block S-matrix operators. In the FCMM, the single block includes inter-regional coupling dynamics, captured by the MC operators. In order to construct the single block scattering matrices with MC operators, the left and right boundary S-matrix operators for the finite block (region II) is defined as: $\mathbf{S}_{II}(z_-) = \left\{\overleftarrow{\mathbf{R}}_{II}(z_-), \vec{\mathbf{T}}_{II}(z_-), \vec{\mathbf{R}}_{II}(z_-), \overleftarrow{\mathbf{T}}_{II}(z_-)\right\}$ and $\mathbf{S}_{II}(z_+) = \left\{\overleftarrow{\mathbf{R}}_{II}(z_+), \vec{\mathbf{T}}_{II}(z_+), \vec{\mathbf{R}}_{II}(z_+), \overleftarrow{\mathbf{T}}_{II}(z_+)\right\}$. The global boundary S-matrix operators are constructed by assembling the local boundary S-matrices at its diagonal part as (Supplement 1 section D).

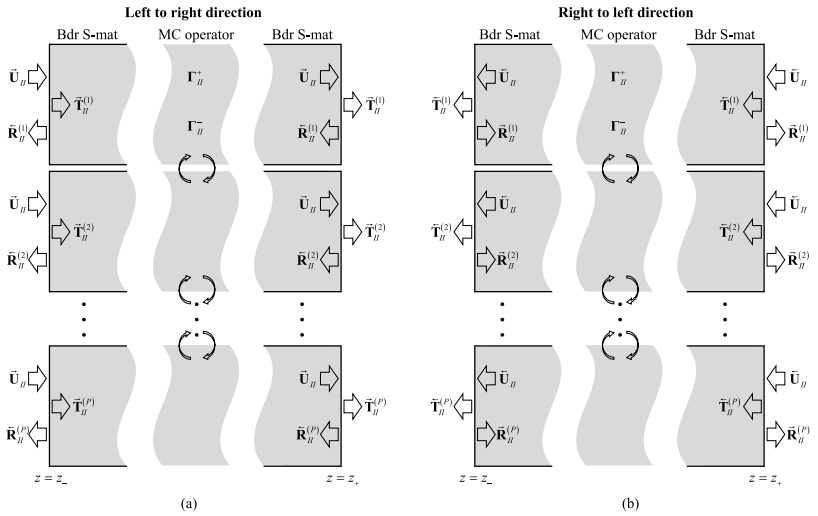

Fig. 4. Single block interconnection with boundary scattering matrix operators and MC operator: (a) for the left-to-right incident wave and (b) for the right-to-left incident wave.

The scattering operators at the interface $z = z_-$ are given by:

$$\overleftarrow{\mathbf{R}}_{II}(z_-) = diag\left(\overleftarrow{\mathbf{R}}_{II}^{(1)}(z_-), \overleftarrow{\mathbf{R}}_{II}^{(2)}(z_-), \cdots, \overleftarrow{\mathbf{R}}_{II}^{(P)}(z_-)\right), \tag{8a}$$

$$\vec{\mathbf{T}}_{II}(z_-) = diag(\vec{\mathbf{T}}_{II}^{(1)}(z_-), \vec{\mathbf{T}}_{II}^{(2)}(z_-), \cdots, \vec{\mathbf{T}}_{II}^{(P)}(z_-)), \tag{8b}$$

Optics EXPRESS

$$\vec{\mathbf{R}}_{II}(z_-) = diag(\vec{\mathbf{R}}_{II}^{(1)}(z_-), \vec{\mathbf{R}}_{II}^{(2)}(z_-), \cdots, \vec{\mathbf{R}}_{II}^{(P)}(z_-)), \tag{8c}$$

$$\overleftarrow{\mathbf{T}}_{II}(z_-) = diag\left(\overleftarrow{\mathbf{T}}_{II}^{(1)}(z_-), \overleftarrow{\mathbf{T}}_{II}^{(2)}(z_-), \cdots, \overleftarrow{\mathbf{T}}_{II}^{(P)}(z_-)\right). \tag{8d}$$

The scattering operators at the interface $z = z_+$ are given by:

$$\overleftarrow{\mathbf{R}}_{II}(z_+) = diag\left(\overleftarrow{\mathbf{R}}_{II}^{(1)}(z_+), \overleftarrow{\mathbf{R}}_{II}^{(2)}(z_+), \cdots, \overleftarrow{\mathbf{R}}_{II}^{(P)}(z_+)\right), \tag{9a}$$

$$\vec{\mathbf{T}}_{II}(z_+) = diag(\vec{\mathbf{T}}_{II}^{(1)}(z_+), \vec{\mathbf{T}}_{II}^{(2)}(z_+), \cdots, \vec{\mathbf{T}}_{II}^{(P)}(z_+)), \tag{9b}$$

$$\vec{\mathbf{R}}_{II}(z_+) = diag(\vec{\mathbf{R}}_{II}^{(1)}(z_+), \vec{\mathbf{R}}_{II}^{(2)}(z_+), \cdots, \vec{\mathbf{R}}_{II}^{(P)}(z_+)), \tag{9c}$$

$$\overleftarrow{\mathbf{T}}_{II}(z_+) = diag\left(\overleftarrow{\mathbf{T}}_{II}^{(1)}(z_+), \overleftarrow{\mathbf{T}}_{II}^{(2)}(z_+), \cdots, \overleftarrow{\mathbf{T}}_{II}^{(P)}(z_+)\right). \tag{9d}$$

Using this global boundary scattering matrix operators and the MC operators, we can derive the left-to-right scattering operators for the finite size single block in Fig. 4(a) as follows:

$$\tilde{\mathbf{\Gamma}}_{a,II}^{(1,1)+}(z) = \mathbf{\Gamma}_{II}^{+}(z)\left(\mathbf{I} - \vec{\mathbf{R}}_{II}(z_-)\mathbf{X}(z_- - z_+)\mathbf{\Gamma}_{II}^{-}(z_-)\overleftarrow{\mathbf{R}}_{II}(z_+)\mathbf{X}(z_+ - z_-)\mathbf{\Gamma}_{II}^{+}(z_+)\right)^{-1}\vec{\mathbf{T}}_{II}(z_-) \tag{10a}$$

$$\tilde{\mathbf{\Gamma}}_{a,II}^{(1,1)-}(z) = \mathbf{\Gamma}_{II}^{-}(z)\overleftarrow{\mathbf{R}}_{II}(z_+)\mathbf{X}(z_+ - z_-)\tilde{\mathbf{\Gamma}}_{a,II}^{(1,1)+}(z_+), \tag{10b}$$

where $\mathbf{X}(z_+ - z_-)$ and $\mathbf{X}(z_- - z_+)$ are the positive and negative propagators between the left and right interfaces (see Supplement 1 section D),

$$\mathbf{X}(z_+ - z_-) = diag(e^{j\beta_v^{(1)+}(z_+ - z_-)}, e^{j\beta_v^{(2)+}(z_+ - z_-)}, \cdots, e^{j\beta_v^{(P)+}(z_+ - z_-)}) \tag{11a}$$

$$\mathbf{X}(z_- - z_+) = diag(e^{j\beta_v^{(1)-}(z_- - z_+)}, e^{j\beta_v^{(2)-}(z_- - z_+)}, \cdots, e^{j\beta_v^{(P)-}(z_- - z_+)}) \tag{11b}$$

The transmission operator is

$$\vec{\mathbf{T}}_{II}^{(1,1)} = \vec{\mathbf{T}}_{II}(z_+)\mathbf{X}(z_+ - z_-)\tilde{\mathbf{\Gamma}}_{a,II}^{(1,1)+}(z_+), \tag{12a}$$

and the reflection operator is

$$\overleftarrow{\mathbf{R}}_{II}^{(1,1)} = \overleftarrow{\mathbf{R}}_{II}(z_-) + \overleftarrow{\mathbf{T}}_{II}(z_-)\mathbf{X}(z_- - z_+)\tilde{\mathbf{\Gamma}}_{a,II}^{(1,1)-}(z_-). \tag{12b}$$

By a similar approach, the right-to-left operators of the finite size single block in Fig. 4(b) are derived. The mode-coupling operators are expressed as:

$$\tilde{\mathbf{\Gamma}}_{b,II}^{(1,1)-}(z) = \mathbf{\Gamma}_{II}^{-}(z)\left(\mathbf{I} - \overleftarrow{\mathbf{R}}_{II}(z_+)\mathbf{X}(z_+ - z_-)\mathbf{\Gamma}_{II}^{+}(z_+)\vec{\mathbf{R}}_{II}(z_-)\mathbf{X}(z_- - z_+)\mathbf{\Gamma}_{II}^{-}(z_-)\right)^{-1}\overleftarrow{\mathbf{T}}_{II}(z_+), \tag{13a}$$

$$\tilde{\mathbf{\Gamma}}_{b,II}^{(1,1)+}(z) = \mathbf{\Gamma}_{II}^{+}(z)\vec{\mathbf{R}}_{II}(z_-)\mathbf{X}(z_- - z_+)\tilde{\mathbf{\Gamma}}_{b,II}^{(1,1)-}(z_-). \tag{13b}$$

The transmission operator of the finite block is

$$\overleftarrow{\mathbf{T}}_{II}^{(1,1)} = \overleftarrow{\mathbf{T}}_{II}(z_-)\mathbf{X}(z_- - z_+)\tilde{\mathbf{\Gamma}}_{b,II}^{(1,1)-}(z_-), \tag{14a}$$

and the reflection operator of the finite block is

$$\vec{\mathbf{R}}_{II}^{(1,1)} = \vec{\mathbf{R}}_{II}(z_+) + \vec{\mathbf{T}}_{II}(z_+)\mathbf{X}(z_+ - z_-)\tilde{\mathbf{\Gamma}}_{b,II}^{(1,1)+}(z_+). \tag{14b}$$

Optics EXPRESS

4. Numerical results

To validate the proposed FCMM theory, the zero-gap multi-slab waveguide systems are numerically analyzed. Numerical simulations are performed by utilizing MATLAB 2022b and MATLAB parallel server. The parallel cluster consists of two workstations with dual Intel 6330N Zeon CPU (@ 2.2 GHz), 2 TB ECC-RDIMM memory (64 GB by 32 EA), and the operating system of Linux Ubuntu 22.04 LTS. The computational nodes are connected using NVIDIA Mellanox connectx-6 HDR/200 GbE adaptor (MCX653106A-HDAT, dual port QSFP56) and NVIDIA Mellanox 200 GbE QSFP56 Direct attach copper cable (MCP1650-V001E30).

As shown in Figs. 5(a) and 5(b), the multi-slab waveguide structure is divided into five local parts. The x-directional and z-directional lengths of the computation domain are set to $60\mu m$ and 40 μm, respectively. The refractive indices of $n_1 = 1$, $n_2 = 1.5$, and $n_s = 0.001$ are assigned to the local parts 1,5 and local parts 2-3, as indicated in Fig. 5(a). This configuration forms a multi-slab waveguide. An obliquely incident Gaussian beam illuminates the left interface of the local part 3 at $z = 0$. The structure of each local region consists of a waveguide embedded in free-space in Fig. 5(a). If an incident angle satisfies the critical angle condition at the boundary between the waveguide and the free-space, the light wave is expected to a total internal reflection. The FCMM analysis result is represented by the field visualization (see Supplement 1 section F) in the structure (Fig. 5(c)) and the evolution of the coupling coefficient function $C_v^{(p)\pm}(z)$ along the z-axis (Fig. 5(d)). In Fig. 5(c), the incident Gaussian beam propagates through the part 3 into the part 4 without any interfacial reflections, confirming the validity of the zero-gap CMT, while it is totally reflected at the interface between the parts 4 and 5 confirming the physical correctness of FCMM. The evolution of the mode coupling operator for the local eigenmodes involved in FCMM reveals the energy exchange relationship of the eigenmodes even under the zero-gap structural condition. According to the evolution of the mode coupling coefficients, we

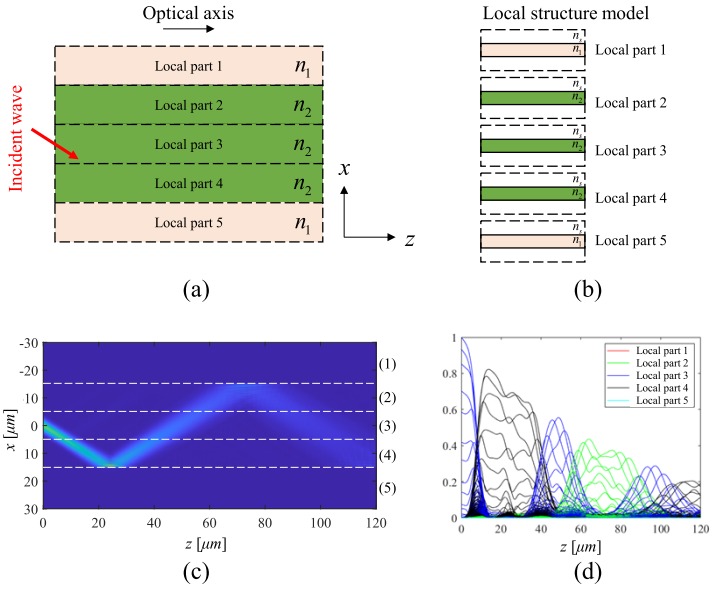

Fig. 5. Mode coupling results of the single block structure obtained by FCMM with 5×1 structural partitioning. (a) Schematic of the 5×1 partitioned slab-waveguide structure, (b) separated 5×1 local structures, (c) FCMM field distribution of a Gaussian incident wave in the slab-waveguide structure, and (d) coupling coefficient function $C_v^{(p)\pm}(z)$ plot quantifying the interaction between eigen-modes of five local parts.

Optics EXPRESS

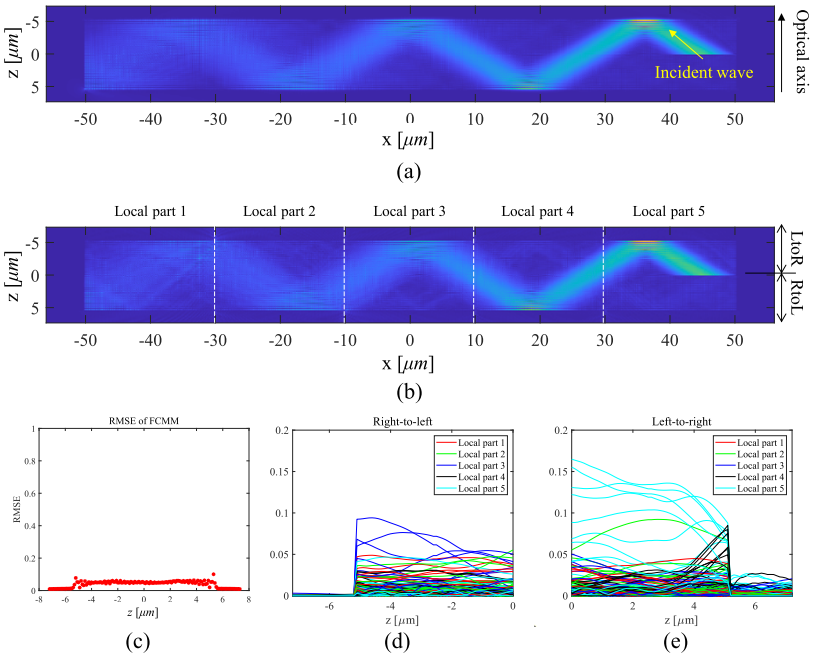

Fig. 6. Numerical results: Bidirectional field visualization of 5×1 multi-layer waveguide with a Gaussian incident wave (Incident wave at $z = 0$). The results are shown for (a) the Fourier modal method (FMM) and (b) the proposed Fourier coupled modal method (FCMM). (c) Root mean square error (RMSE) of the result of FCMM to the reference result of FMM along the z-axis. and the coupling coefficient function plots of (d) the right-to-left (RtoL) part in the negative z-region and the (e) the left-to-right (LtoR) part in the positive z-region.

observe energy exchange among the mode coupling coefficients of the parts 2-4 are exchanging energy, while the mode coupling coefficients of the parts 1 and 5 remain zero, indicating that no modes are excited in the low-refractive index parts 1 and 5.

Figures 6 and 7 display the bidirectional FCMM field distribution (see Supplement 1 section E), along with a comparison between FMM and FCMM [15]. In the numerical results shown in Fig. 6, the truncated order of global structure is 660, and the truncated order of local part is 180. Consequently, in the local structure, the dimension of the single eigenvalue problem in FCMM is reduced to 722×722, which is significantly smaller compared to the single eigenvalue problem dimension of $2{,}642 \times 2{,}642$ in the conventional FMM. In terms of peak memory usage (PMU) required for solving the single eigenvalue problem, the PMU of FMM is 1,156 MB, whereas the PMU for each local component in FCMM is reduced to 83 MB, approximately $1/14$ of the memory requirement for FMM. For FMM analysis on the global domain in Fig. 6(a), it is consisted of the total period along the x-axis T_x, $100\,\mu m$, the thickness along the z-axis T_z, $14.6\,\mu m$, the refractive index n_1, 1.9, and the refractive index n_2, 1.5. For FCMM, the total structure is divided into 5×1 parts with the local period $T_{x,local}$ of each part, $20\,\mu m$.

Figure 6(a) illustrates the FMM field visualization result, whereas Fig. 6(b) presents the FCMM results of 5×1 spatial partitioning. In Fig. 6(b), it can be observed in the presented field distribution that the field is transmitted through the two-layer boundaries for n_1 without any interfacial reflection. The root mean square error (RMSE) of the FCMM result compared to the FMM result along the z-axis is presented in Fig. 6(c). The RMSE is 0.0451 for the total field distribution and 0.0519 of the internal waveguide field distribution. The evolution of the coupling coefficient functions of FCMM field are presented in Figs. 6(d) and 6(e), which present the

Optics EXPRESS

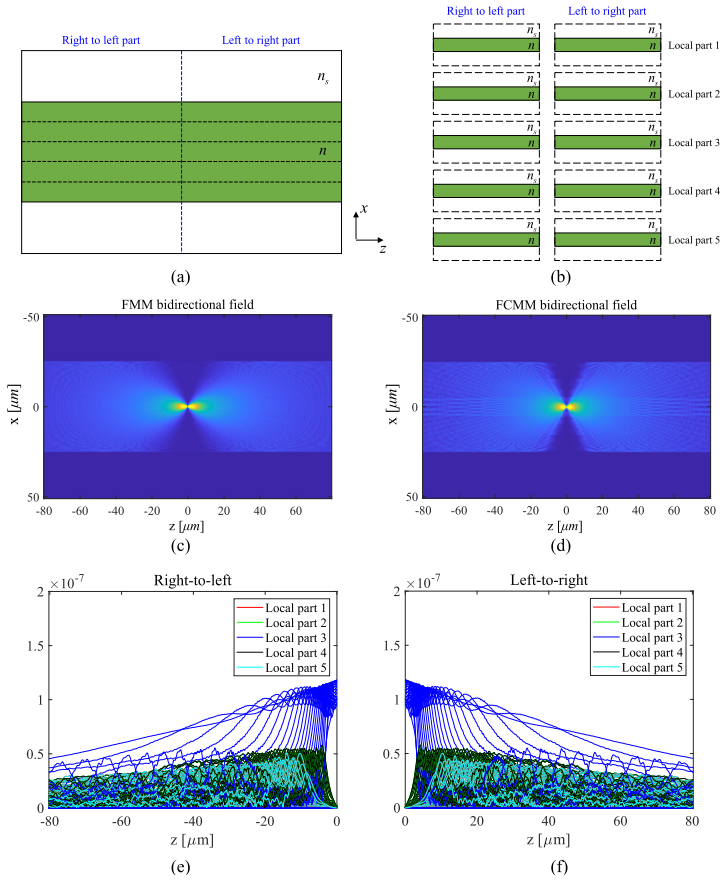

Fig. 7. Bidirectional dipole field simulation: (a) Structure model in the global domain, (b) local part partitioning, (c) FMM field distribution, (d) FCMM field distribution for a dipole source, and the coupling coefficient function evolutions of the local modes in (e) the RtoL part and (f) the LtoR part.

modal energy exchanges among the negative z-directional (right-to-left) modes and the positive z-directional (left-to-right) modes. The numerical results of FCMM qualitatively demonstrate an accurate physical representation of the coupling phenomenon in the transverse region, while the quantitative evaluation reveals a notably low RMSE. Figure 7 presents the guided field from a point source in the single waveguide. As the global domain in Fig. 7(a) size along the x-axis is $100\,\mu m$, the local domain in Fig. 7(b) is the 5×1 divided part with the local period $T_{x,local}$, $20\,\mu m$. The width of waveguide is $50\,\mu m$, with each divided waveguide of the local region being $10\,\mu m$. The refractive index of the waveguide is 1.5, while the refractive index of the surrounding region is virtually set to 0.001 for total internal reflection of a point source. The evolution of the coupling coefficient functions of FCMM field are presented in Figs. 7(e) and 7(f), which are for the right-to-left incident direction and the left-to-right incident direction. In FMM, the global truncation order is set to 400, while in FCMM, the local truncation order of x-axis is 80. As a result, in the local structure, the dimension of the single eigenvalue problem in the FCMM (Fig. 7(d)) is reduced to 322×322, which is compared to the single eigenvalue problem dimension of $1{,}602 \times 1{,}602$ in the conventional FMM (Fig. 7(c)). Regarding the peak memory usage (PMU) required to the process of solving the single eigenvalue problem, the PMU of FMM is 424 MB, while the PMU for each local part in FCMM is reduced to 16 MB, approximately $1/26$ of the FMM requirement.

Optics EXPRESS

5. Concluding remarks

In conclusion, we propose the Fourier coupled modal method (FCMM), which enables the dimensional reduction of large-scale eigenvalue problem into multiple reduced-dimension eigenvalue problem by spatially partitioning the target structure. This approach facilitates computational parallelization. In this paper, we derived the core mathematical model of FCMM and presented numerical results validating the 2D algorithm as a preliminary step toward developing a three-dimensional (3D) parallel computation method. In the future research of 3D FCMM, we aim to verify FCMM's capability to handle eigenvalue problems of a scale that the conventional Fourier modal method (FMM) cannot process on a single computer, leveraging parallel computer clusters This study revealed that the memory required to solve eigenvalue problem in FCMM can be significantly reduced, an important finding for the advancement of 3D FCMM. From the perspective of applied mathematics, a large-scale parallel solver for general non-symmetric complex non-Hermitian matrices has not been fully developed. The FCMM represents a step toward overcoming this fundamental mathematical challenge by extending coupled mode theory (CMT) to FMM. Our ultimate goal is to develop FCMM into a practical and efficient simulation and analysis tool for complicated 3D photonic structures such as display devices, waveguide devices, and photonic integrated circuits.

Funding. Samsung Display; National Research Foundation of Korea (2022R1A2C1012559).

Disclosures. The authors declare no conflicts of interest.

Data availability. Data underlying the results presented in this paper are not publicly available at this time but may be obtained from the authors upon reasonable request.

Supplemental document. See Supplement 1 for supporting content.

References

1. A. Taflove and S. C. Hagness, *Computational electrodynamics: the finite-difference time-domain method* (Artech house, 2005).
2. O. C. Zienkiewicz, R. L. Taylor, and J. Z. Zhu, *The Finite Element Method: Its Basis and Fundamentals* (Elsevier, 2005).
3. B. Szabó and I. Babuška, "Finite element analysis: Method, verification and validation," (Wiley, 2021).
4. P. Lalanne and E. Silberstein, "Fourier-modal methods applied to waveguide computational problems," Opt. Lett. **25**(15), 1092–1094 (2000).
5. H. Kim, I.-M. Lee, and B. Lee, "Extended scattering-matrix method for efficient full parallel implementation of rigorous coupled-wave analysis," J. Opt. Soc. Am. A **24**(8), 2313–2327 (2007).
6. H. Kim and B. Lee, "Mathematical modeling of crossed nanophotonic structures with generalized scattering-matrix method and local Fourier modal analysis," J. Opt. Soc. Am. B **25**(4), 518–544 (2008).
7. H. Kim, J. Park, and B. Lee, *Fourier Modal Method and Its Applications in Computational Nanophotonics* (CRC Press, 2017).
8. M. Alhubail and Q. Wang, "The swept rule for breaking the latency barrier in time advancing PDEs," J. Comput. Phys. **307**, 110–121 (2016).
9. J. Kestyn, E. Polizzi, and P. T. Peter Tang, "Feast Eigensolver for Non-Hermitian Problems," SIAM J. Sci. Comput. **38**(5), S772–S799 (2016).
10. A. Horning and A. Townsend, "FEAST for differential eigenvalue problems," SIAM J. Numer. Anal. **58**(2), 1239–1262 (2020).
11. W.-P. Huang, "Coupled-mode theory for optical waveguides: an overview," J. Opt. Soc. Am. A **11**(3), 963–983 (1994).
12. D. Marcuse, "Coupled power equations for lossy fibers," Appl. Opt. **17**(20), 3232–3237 (1978).
13. H. A. Haus and W. Huang, "Coupled-mode theory," Proc. IEEE **79**(10), 1505–1518 (1991).
14. A. Yariv, "Coupled-mode theory for guided-wave optics," IEEE J. Quantum Electron. **9**(9), 919–933 (1973).
15. S. Park, J. Hahn, and H. Kim, "Fourier modal method for optical dipole radiation in photonic structures," Curr. Opt. Photon. **5**, 597–605 (2021).
16. A. V. Chebykin, A. A. Orlov, A. V. Vozianova, *et al.*, "Nonlocal effective medium model for multilayered metal-dielectric metamaterials," Phys. Rev. B **84**(11), 115438 (2011).
17. M. Coppolaro, G. Castaldi, and V. Galdi, "Anomalous light transport induced by deeply subwavelength quasi-periodicity in multilayered dielectric metamaterials," Phys. Rev. B **102**(7), 075107 (2020).
18. Z. Wen, H. Xu, W. Zhao, *et al.*, "Nonlocal effective-medium theory for periodic multilayered metamaterials," J. Opt. **23**(6), 065103 (2021).